

## DETAILED DESIGN AND TECHNO-ECONOMIC ASSESSMENT OF A TRANSCRITICAL CO<sub>2</sub>-BASED CARNOT BATTERY SYSTEM FOR LONG DURATION ENERGY STORAGE

**Simone Girelli**  
Politecnico di Milano  
Milan, Italy

**Ettore Morosini**  
Politecnico di Milano  
Milan, Italy

**Dario Alfani\***  
Politecnico di Milano  
Milan, Italy  
email: dario.alfani@polimi.it

**Marco Astolfi**  
Politecnico di Milano  
Milan, Italy

### ABSTRACT

Long duration energy storage systems with 8-12 hours of capacity are one of the best options to reduce the increasing curtailment of renewable energy, being able to provide intra-day storage. Among those systems, Carnot batteries operating with CO<sub>2</sub> can be a promising solution due to the relatively high round trip efficiencies (up to 60%), being site-independent, including the possibility to store and sell both cold and hot thermal power in addition to electricity. In this work, the detailed sizing of the main components of a CO<sub>2</sub> Carnot battery is proposed: in particular, an interesting and promising feature of the system is represented by in the adoption of the same heat exchangers during the charging and the discharging phase, while the cold and hot storage systems are inspired by the commercial solution proposed by Echogen Power Systems. Specifically, the hot storage consists of two heat transfer fluid loops: a pressurized water loop and a diathermic oil loop, requiring two different insulated tanks, whereas the cold storage is based on an ice slurry tank. A routine in MATLAB has been developed to properly design the system and optimize its main variables to maximize the round-trip efficiency and minimize the storage costs, but also including the calculation of the levelized cost of storage. The battery is simulated with a cold storage at 0°C and hot storage between 71.6°C and 293.7°C, with the cycle maximum pressure of 250 bar and a round-trip efficiency of 54.6%. The specific capital cost of the system is 2033 €/kW<sub>el, ch</sub>, with the largest share being the storage systems. The levelized cost of storage is estimated around 0.1 and 0.3 €/kWh, depending on the electricity selling price, and a relatively large internal temperature difference in the hot storage (20°C) is suggested for these systems.

### 1. INTRODUCTION

In recent years, the electrical production from non-dispatchable renewable energy sources has soared, mainly thanks to the significant capital cost reduction achieved by solar photovoltaic panels and the wind turbines, driven by significant investments in energy policies implemented by many countries with the goal of pushing towards a more decarbonized society.

\* corresponding author(s)

However, integrating variable renewable energy sources (VRES) into the existing electrical grid introduces significant challenges mainly due to the intermittent nature of solar and wind power which results in a frequent mismatch between renewable energy generation and electricity demand profile and consequent curtailment as already experienced by California and China [1], [2]. For this reason, in the last decade the interest in efficient and cost-effective energy storage solutions has grown considerably, becoming one of the crucial research topics in both the academic and industrial fields, since such systems could also provide critical ancillary services to the electrical grid, such as frequency regulation and peak load management [3].

Among the different energy storage solutions commercially available, pumped hydro energy storage (PHES) and battery energy storage systems (BESS) have emerged as the most mature and widely deployed solutions. In particular, PHES is the main player in the global energy storage market, accounting for 94% of the world electrical storage installed capacity. This technology benefits from its proven reliability, its ability to scale up to GW range, its high round trip efficiency (RTE), ranging between 65% and 85%, and its low levelized cost of storage (LCOS) [4]. However, due to the high capital cost and an intrinsic dependency on specific topographical characteristics the potential for an increase in installed capacity is limited in many countries. On the other hand, BESS do not require specific geographical requirements, and they can be deployed both in small-scale residential applications and large utility-scale installations. Thanks to its flexibility and rapid deployment capability, BESS has emerged as a key solution for short-term energy storage and grid stabilization. Nevertheless, battery storage system relatively shorter lifespan, higher maintenance costs [4], and dependency on critical minerals such as lithium, cobalt, and nickel pose significant issues. In addition, supply chain vulnerabilities, geopolitical tensions, and ethical concerns related to mining practices have raised questions about the sustainability and reliability of battery supply chains [5].

In addition to these established storage technologies, emerging solutions like compressed air energy storage (CAES) or liquid air energy storage (LAES) are gaining commercial

interest, such as in the case of companies such as Hydrostor [6] and Highview Power [7]. Both CAES and LAES require not only the accumulation of energy in thermal energy storage, but also the storage of the working fluid as a gas at high pressure (CAES) or as a liquid (LAES). Carnot batteries, on the contrary, are based on the adoption of closed thermodynamic cycles in both charging (heat pump) and discharging (power cycle) phases and thus they require only the storage of heat. This feature allows to potentially simplify the system and reduce its size for long duration energy storage applications.

Carnot batteries based on transcritical CO<sub>2</sub> cycles are currently developed by MAN Energy Solutions [8] and Echogen Power Systems [9]. MAN is working on a low temperature system able to provide also heating and cooling services in addition to electricity. Differently, Echogen recently partnered with Westinghouse Electric Company for the commissioning of a large scale LDES system in Alaska [10] and is currently studying a CO<sub>2</sub>-based PTES using water and diathermic oil as hot storage media.

In recent years several studies have investigated this type of system [11], [12], [13]. Nevertheless, there is a lack of literature studies where detailed component sizing and techno-economic evaluations are carried out. To fill this research gap, in this work the system components have been preliminary sized and the techno-economic evaluation of the performance of a transcritical CO<sub>2</sub>-based Carnot battery system was carried out, estimating its LCOS.

## 2. SYSTEM DESCRIPTION

In this work, a large scale transcritical CO<sub>2</sub> Carnot battery is analyzed for daily storage applications and focusing on a size of 50 MW<sub>el,ch</sub>/10 h of storage. In particular, the investigated system consists of:

- A cold storage consisting of an ice slurry tank integrated with a shell & tube heat exchanger.
- A hot storage consisting of two thermal loops and two thermocline tanks, one employing water both as heat transfer fluid (HTF) and storage media and the other one employing Therminol VPI as HTF and using rocks (Limestone or other low-cost minerals/rocks\*) as storage medium.
- A transcritical CO<sub>2</sub> system that can operate in charging phase as a heat pump and in discharging phase as a power cycle, adopting the same heat exchangers in both phases while compressor and turbine being based on turbomachinery have to be different components.

The adoption of heat exchangers common to both operating modes allows to a significant reduction of the required equipment and system costs while, on the other hand, it introduces a more complex operation of one of the two phases, since the components cannot be designed ad-hoc for both operating conditions and also requires the development of dedicated numerical iterative routines to determine the discharge cycle operation once the components are designed in charging mode, as better explained in detail in section 3.2.

The T-s (temperature – specific entropy) diagrams of the two operating modes are reported in **Figure 1**. During the charging phase, saturated vapor is first superheated in a recuperator (1→2) before being pressurized by the compressor (2→3). The high temperature CO<sub>2</sub> is then cooled down transferring heat to the two hot thermal storage loops (3→4). Subsequently, the CO<sub>2</sub> is further cooled down in the recuperator (4→5) where the low-pressure CO<sub>2</sub> is heated up (1→2). The high-pressure cooled CO<sub>2</sub> is then expanded into a two-phase flow expander (5→6) down to the evaporator pressure, recovering part of the compression work and thus enhancing the heat pump COP. Finally, the cold storage thermal energy is used to evaporate the working fluid (6→1), closing the cycle.

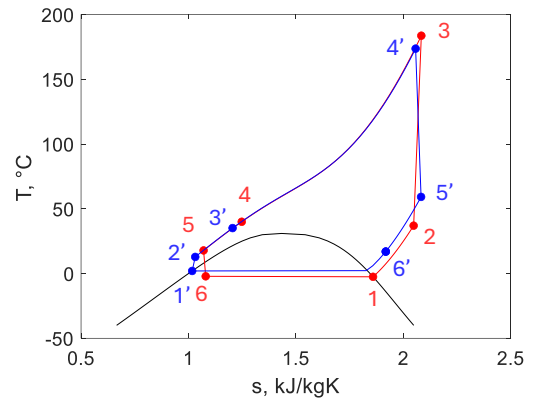


**Figure 1** T-s diagram of the charging (red) and discharging (blue) phase of the Carnot battery, superimposed

During the discharging phase, the cycle operates in the opposite direction. Saturated liquid is pressurized by a pump (1'→2') and pre-heated in the recuperator (2'→3') before entering in the hot thermal storage section. Here, the heat stored during the charging phase is used to increase the CO<sub>2</sub> temperature (3'→4') before being expanded through a turbine (4'→5'). The low-pressure CO<sub>2</sub> is then cooled in the recuperator (5'→6') and eventually in the condenser, where energy is released to the cold storage media (6'→1'). If the temperature of CO<sub>2</sub> in point 6' is higher than the ambient, a CO<sub>2</sub> cooler is considered before the condenser with the scope to release heat to the ambient and reduce the heat released to the cold storage.

Being the two cycles operating between similar temperature and pressures and with real components the power consumption in charging phase is inevitably higher than the power produced in discharge thus leading to RTE lower than 100%. Considering the assumption that the thermal energy stored in the hot storage during the charging phase is then completely exploited by the discharging one, it is required to extract heat from the cold storage to ensure its energy balance (see Eq (1)) where  $Q_{amb}^{dh}$  is positive only if the additional CO<sub>2</sub> cooler can be implemented.

$$W_{net}^{ch} - W_{net}^{dh} - Q_{amb}^{dh} = Q_{cold}^{dh} - Q_{cold}^{ch} = \Delta Q_{cold}^{balance} \quad (1)$$

The additional heat released to cold storage during condensation in power cycle mode ( $\Delta Q_{cold}^{balance}$ ) is removed with

\* Selection of the solid and the oil shall be based on experimental evaluation of their chemical compatibility

an external chiller as already proposed in previous studies [11], [12], [13].

The resulting overall plant scheme is reported in **Figure 2**, showcasing the HX and the thermal energy storage of the system employed during both phases.

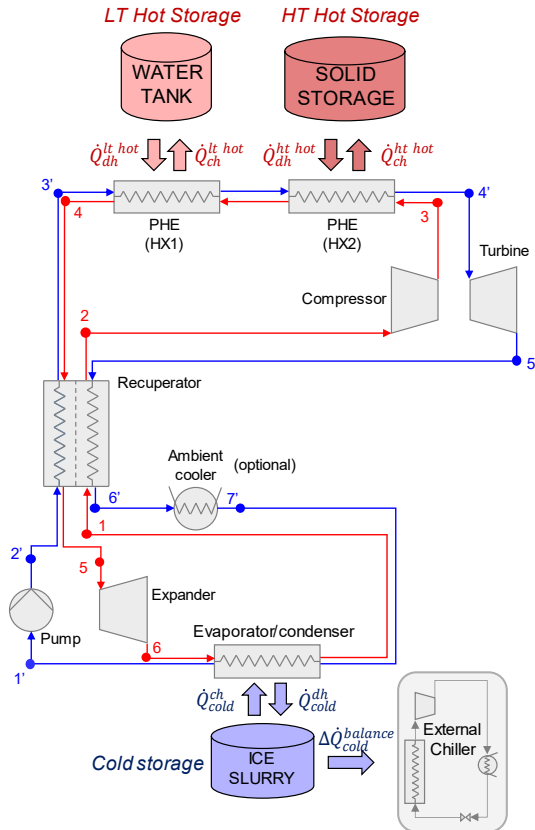


**Figure 2** Overall plant scheme. The red line path represents the charging phase process (heat pump), while the blue one represents the discharging one (power cycle)

Two different HTF loops are needed for the hot storage because the CO<sub>2</sub> temperature can be above 250°C in the proposed configuration thus exceeding the maximum achievable temperature of a water storage limited at 150°C when adopting a limited pressurization. Consequently, Therminol VP1 has been adopted as HTF in the high temperature region, with solid limestone as storage material to limit the amount of flammable and expensive fluid. Additionally, the use of two different hot storage loops allows to better match the non-linear temperature profile of CO<sub>2</sub> during the heat transfer process, thus lowering the temperature difference between the charging and discharging maximum temperature and increasing the system RTE, as it was proved in previous studies [12].

The hot storage system is detailed in Figure 3, where both the water and the Therminol loops are reported. During the charging phase the hot CO<sub>2</sub> released by the compressor first heats up the Therminol VP1 (HX2) which is then conveyed to the packed bed tank where thermal energy is released to the solid granular material (limestone). Afterwards, the partially cooled working fluid is sent to HX1, heating up the water that is directly

stored in a water tank. During the discharging phase the described process is reversed and the direction of all the streams of **Figure 3** is inverted.

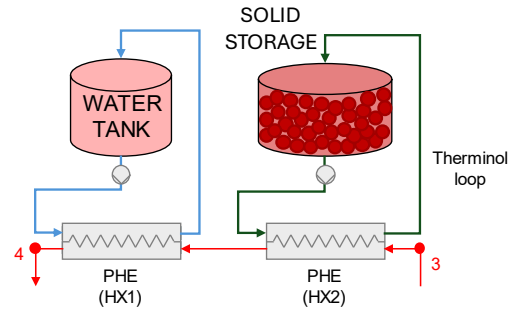


**Figure 3** Scheme of the hot storage scheme operation during the charging phase

### 3. METHODS

The routine proposed to define an optimized configuration of the Carnot battery with shared HXs is reported in the flowchart of **Figure 4**. Calculations are based on a set of assumptions and dedicated numerical scripts for HXs design (Section 3.1) and carried out by means of two separate and subsequent steps: first, the charging and discharging cycles are simulated and optimized by maximizing the RTE (Section 3.1), then, the model iteratively defines the Hot storage configuration that minimizes the storage costs (Section 3.2).

#### 3.1. Assumptions and HXs modelling

To complete the definition of the plant scheme and its characteristics, a set of assumptions on the different components and boundary conditions (i.e. temperatures and pressures) are defined in **Table 1**. Preliminary analysis showed that increasing the maximum pressure of the system leads to an increase of the RTE, due to the larger temperature difference between the cold and hot storage, and of the energy density (ED), due to: (i) the increased CO<sub>2</sub> temperature variation between in the energy transfer with the hot storage (3→4 and 3'→4') that allows to reduce the amount of HTF and consequent water and packed bed tank sizes and (ii) the increase of specific work in both operating modes allowing to design smaller components. Consequently, in this work, the maximum pressure of both cycles has been fixed to 250 bar as it is usually considered as the technical limit for CO<sub>2</sub> cycles [14]. **Table 1** reports the set of characteristics for the system in charging phase (for the heat pump, evidenced in red in **Figure 2**), such as pressure drop and internal temperature differences: these correspond to the minimum number of assumptions necessary to univocally carry out the design of all the HXs. To precisely compute the HXs area, discretized 1-D models for the design and preliminary sizing of the HX are implemented in MATLAB. The recuperator is modelled according to the approach of Dostal [15] as a printed circuit heat exchanger (PCHE), while the hot storage section heat exchangers are modelled assuming a shell and tube geometry with tubes of internal diameter of 20 mm and a constant shell side convective heat transfer coefficient (HTC) of 1000 W/m<sup>2</sup>/K for Therminol and 7500 W/m<sup>2</sup>/K for water [16].

**Table 1.** Main assumptions for cycles simulation

Parameter	Value
Charging/Discharging phase maximum pressure	250 bar
Turbine isentropic efficiency	90%
Pump isentropic efficiency	75%
Compressor isentropic efficiency	85%
Expander isentropic efficiency	80%
Minimum $\Delta T_{ch-dh\ HOTS}$	10°C
Cold storage temperature	0°C
Evaporator minimum $\Delta T$ (Charging phase)	3°C
Recuperator minimum $\Delta T$ (Charging phase)	3°C
$\Delta p$ Recuperator - Hot Side (Charging phase)	2%
$\Delta p$ PHE (Charging phase)	1%
$\Delta p$ Condenser (Charging phase)	1%
Chiller 2 <sup>nd</sup> Law Efficiency	45%
Ambient temperature	15°C

Finally, a shell and tube architecture is considered also for the low pressure evaporative/condensative heat exchanger, where a fixed external HTC of 5000 W/m<sup>2</sup>/K [17] has been considered for the iced slurry mixture of water and glycol. Employing small fractions of glycol does not significantly alter the phase change temperature, while ensuring an easier slurry formation [18]. Additionally, adopting small maximum ice fraction at low glycol fraction does not significantly impact the temperature glide in solidification [19]. The chiller electrical consumption is computed considering the chiller 2<sup>nd</sup> law efficiency reported in **Table 1** that results in a COP of around 8.2 for the ambient temperature considered in this work. Hot storage HXs design is carried out by fixing a minimum difference between the CO<sub>2</sub> temperature profiles on the charging and discharging phase

( $\Delta T_{ch-dh\ HOTS}$ ). The system is simulated accounting for the thermodynamic and transport properties of the working fluid as computed by REFPROP Version 10 [20]. The set of correlations employed to compute the CO<sub>2</sub> heat transfer coefficients and frictional pressure drop ( $\Delta p$ ) in single phase, condensation and evaporation are listed in **Table 2**.

**Table 2.** Correlations to compute the HTC and frictional pressure drop in the HX 1-D models

CO <sub>2</sub> Conditions	HTC Model	$\Delta p$ Model
Evaporation	Liu and Winterton [21]	Friedel [22]
Condensation	Cavallini [23]	Friedel [22]
Single phase	Gnielinski [24]	Chen [25]

**3.2. Design routine for the Carnot battery with shared HX**

The concept behind the simulation strategy has been already proposed in literature [26] for ORC based Carnot Batteries and it consists in designing all the heat exchangers during the charging phase and then iteratively solve the discharging phase by finding the thermodynamic conditions that provide the same HX geometry.

The Carnot battery design is defined by considering as input the characteristics reported in **Table 1** and using the CO<sub>2</sub> temperature at the inlet of the hot storage section in the heat pump mode ( $T_4$ ) as the sole optimization variable. Initially, with a guess value of cold side pressure drop in the recuperator ( $\Delta p_{PCH}^{COLD, ch}$ ) in the heat pump mode, all the thermodynamic conditions of the cycle are computed, including the heat pump mass flow rate necessary to achieve the target power.

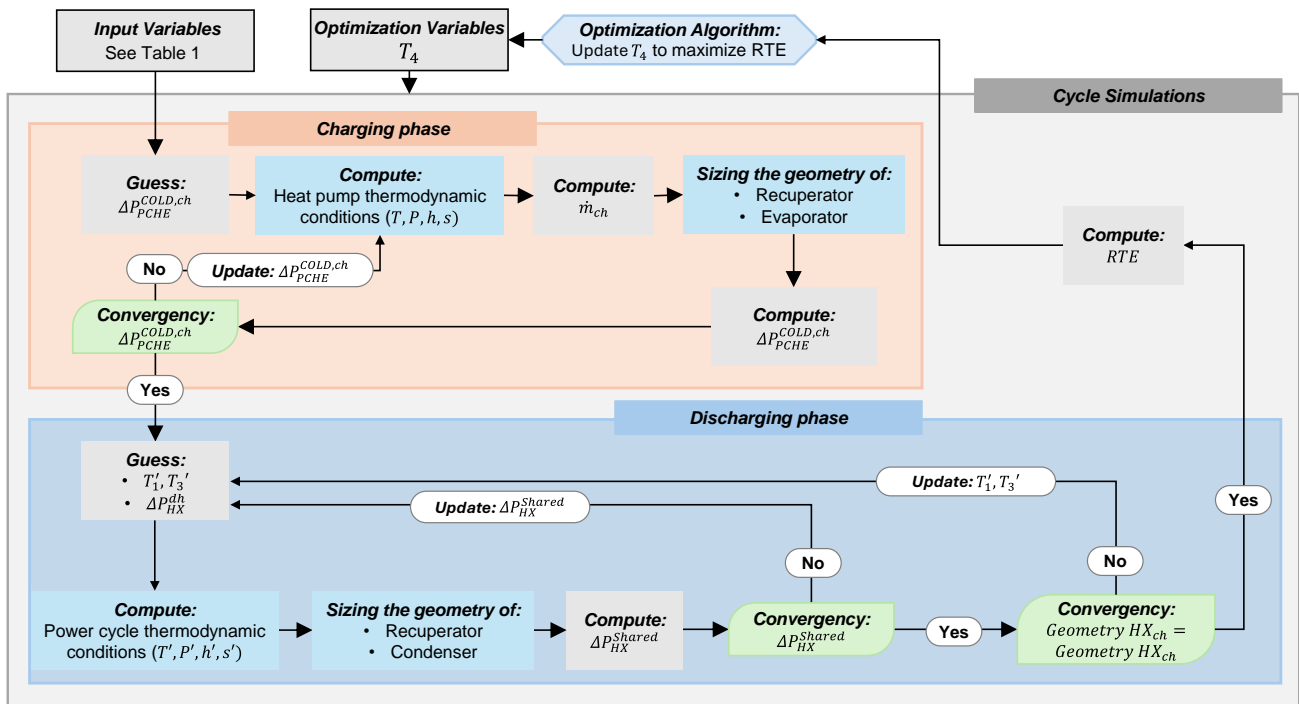


**Figure 4** Flowchart for the design and optimization of the charging and discharging phase of the CO<sub>2</sub> Carnot battery

Subsequently, the resulting  $\Delta p_{PCHE}^{COLD, ch}$  of the modelling tool is compared to the initial guessed value, updating it until convergency. After the heat pump mode is computed and all the HXs have been sized, the analysis switches to the power cycle modelling with a guess value for the minimum temperature ( $T_1$ ), the temperature at hot storage section inlet ( $T_3$ ) and all the pressure drops in the HXs. The numerical solution of the power cycle is obtained by finding the mass flow rate that leads to a target  $\Delta T_{ch-dh_{HOT TES}}$  of  $10^\circ\text{C}$ . Afterwards, the sizing of the recuperator and the condenser is repeated, updating the guessed values of pressure drop ( $\Delta p_{HX}^{dh}$ ) to reach convergency. Eventually, the guessed values of  $T_1$  and  $T_3$  are iteratively updated until the computed HXs heat transfer area matches the one of the charging phase. An external optimization algorithm based on the patternsearch method is employed to identify the  $\text{CO}_2$  temperature at hot storage section outlet of the charging phase ( $T_4$ ) that maximizes the RTE.

### 3.3. Design routine for the hot storage

As the thermodynamic conditions of the  $\text{CO}_2$  are completely defined by the previous optimization procedure, only the temperature profiles of the two hot storage media are yet to be evaluated. The methodology depicted in the flowchart of **Figure 5** is adopted to minimize the hot storage investment cost by optimizing the inlet temperature of the water ( $T_a$ ), the outlet temperature of the thermal oil ( $T_c$ ) and the  $\text{CO}_2$  intermediate temperature on the hot side ( $T_d$ ). The hot storage sizing procedure starts by guessing the outlet water temperature ( $T_b$ ) and inlet oil temperature ( $T_c$ ).

The two separate HXs are hence designed considering the working fluid conditions during the charging phase (heat pump), computing the number and length of the tubes of the two shell and tubes HXs. Afterwards, the same design procedure is repeated for the discharging phase and the process is repeated until convergency is reached on the tube overall length and heat transfer surface for both HXs, updating the variables  $T_b$  and  $T_c$ .

The overall hot TES cost is then estimated by computing the contribution of the system tanks, the storage media, HTF and of the two shell and tubes HXs, using the cost correlations reported in section 4.1.

The patternsearch optimization algorithm implemented in MATLAB [27] is employed to find out the set of temperatures  $T_a$ ,  $T_c$  and  $T_d$  able to minimize the capital cost of the whole storage section, identifying the Carnot battery configuration characterized by the maximum RTE and minimum cost of the hot TES.

To avoid technically unfeasible solutions, the maximum water temperature was limited to  $150^\circ\text{C}$  to avoid the need for excessive storage pressures. Similarly, a minimum temperature of  $100^\circ\text{C}$  was assumed for Therminol VPI to always ensure sufficiently high oil viscosity.

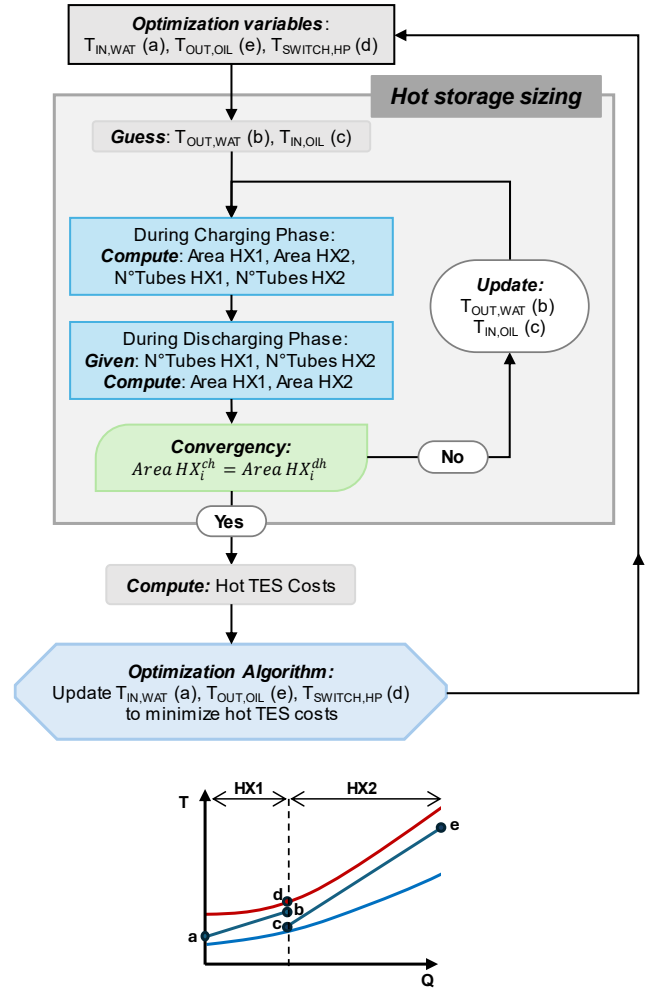


**Figure 5** Details on the methodology for the economic optimization of the dual-loop hot storage system

## 4. ECONOMIC ANALYSIS AND LEVELIZED COST OF STORAGE CALCULATIONS

### 4.1. Cost correlations

To evaluate the total capital expenditures (CAPEX) of the plant, each component cost is evaluated based on the cost correlation listed in **Table 3**. All costs have been actualized based on the Chemical Engineering Plant Cost Index (CEPCI) of 2023 (800.8). The reference year of all the correlations, as well as the corresponding CEPCI value are reported in **Table 3**. A cost of water equal to  $1 \text{ €/m}^3$ , a cost of Therminol VPI of  $2.5 \text{ €/kg}$  [24] and a cost of limestone of  $0.016 \text{ €/kg}$  [25] have been assumed. Additionally, the cold storage system has been sized assuming a maximum ice fraction of 20% [19], while the two hot storage are sized assuming an oversize of 20% to avoid thermocline breakthrough and assuming a void fraction of 0.4 for the solid storage. A specific chiller cost of  $120 \text{ €/kW}_{th}$  based on vendor data [28] for large scale chiller and the cost reported in [29] after actualization.

**Table 3** Capital cost correlations adopted for the system

Component	Correlation	Year	CEPCI
Compressor	Weiland [30]	2017	567.5
Turbine	Weiland [30]	2017	567.5
Pump	Carlson [31]	2016	541.7
Expander	Astolfi [16]	2013	567.3
Recuperator (PCHE)	Weiland [30]	2017	567.5
Shell & tube HX	Astolfi [16]	2013	567.3
High temperature storage	Manzolini [32]	2019	607.5
Low temperature and cold storage	Thermoflex	2020	596.2

4.2. LCOS calculation

Once the CAPEX is estimated, the LCOS of the system can be computed with Eq (2), where operation and maintenance (O&M) costs are computed as 1% of the overall CAPEX [33]. In the equation,  $E_p$  and  $E_s$  are the purchased and sold electricity (in  $MWh_{el}$ ) respectively,  $p_{el}$  is the cost of the purchased electricity (in  $\$/MWh_{el}$ ),  $i$  is the discount rate (assumed equal to 5%) and  $n$  is the plant lifetime (assumed equal to 30 years). A parametric analysis, varying the number of charging/discharging cycles, has been assessed for different values of cost of purchased electricity, to provide an insight on how these two parameters quantitatively affect the LCOS of the system. For the sake of simplicity all the thermal losses of the storage systems have been neglected and it has been assumed that the system always works in nominal conditions. Thus, for each cycle the Carnot battery is completely charged by  $500 MWh_{el}$ , while for each discharging cycle  $E_s$  is computed multiplying this value for the computed system RTE.

$$LCOS = \frac{CAPEX \cdot CRF + O\&M + E_p \cdot p_{el}}{E_s} \quad (2)$$

$$CRF = \frac{i(i+1)^n}{(i+1)^n - 1}$$

5. RESULTS

The T-s diagrams of the optimized solution for the assumptions reported in Table 1 are reported in Figure 6. In particular, the optimization process leads to an optimal  $T_4$  equal to  $78.5^\circ C$  and a maximum temperature  $T_3$  of  $293.8^\circ C$ , achieving an RTE of 54.6%.

The resulting hot storage system is reported in the T-Q diagram of Figure 7, including all the most relevant temperatures. It is evident that the optimization process led to an optimal outlet water temperature close to the imposed limit of  $150^\circ C$ .

Since the water price is way lower than Therminol VP1, the optimizer selects to employ water up to its application limit, increasing the amount of water while reducing the amount of more expensive Therminol VP1. Additionally, Figure 7 proves the need for two separate storage loops, as employing a single loop of heat transfer fluid would clearly lead to a crossing of the temperature profiles either in the charging or in the discharging phase.

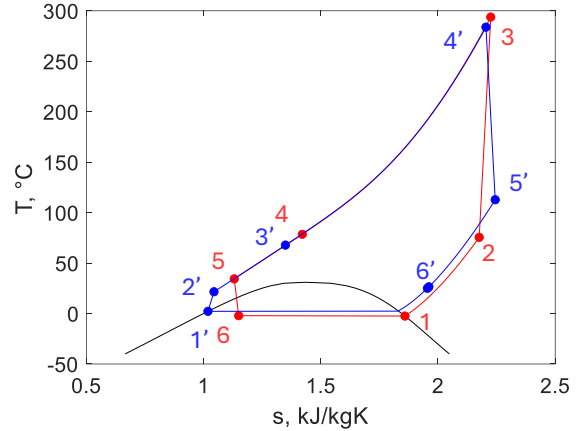


Figure 6 T-s diagram of the optimized Carnot battery for the input variables as reported in Table 1

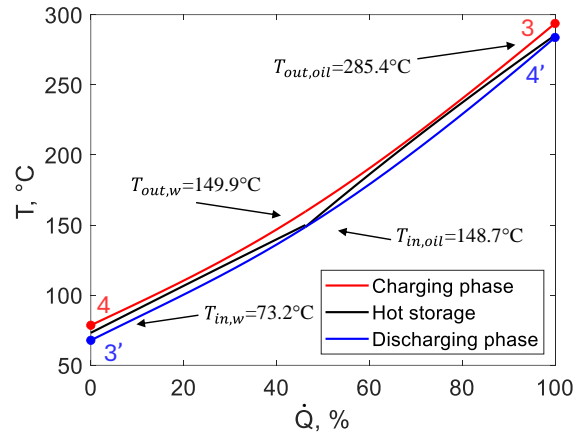
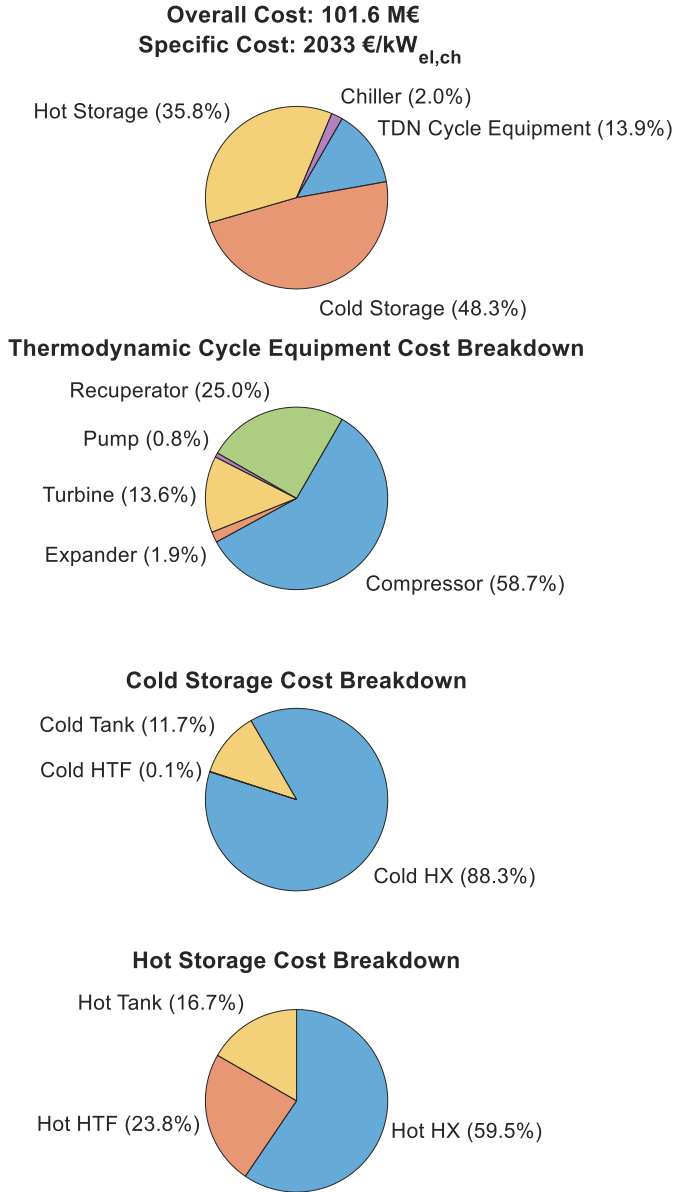


Figure 7 T-Q diagram of the optimized hot storage system for the input variables as reported in Table 1

To give more insights into the optimization results, the total cost of the system and the share of each component is reported in Figure 8. It is evident from the first pie chart that the equipment related to the thermodynamic (TDN) cycles (i.e., turbomachinery and recuperator) accounts only for a limited part of the total costs when compared to the hot and cold storage system, inclusive of their HXs. Additionally, Figure 8 also shows that the greatest portion of both hot and cold storage is represented by the shell & tube HXs. This is directly related to the little internal  $\Delta T$  of the two heat exchangers reported in Figure 7, that leads to high HX surface area and cost, demonstrating the importance of using the same HXs in both charging and discharging phase. If separate HXs dedicated to each phase would be employed, their total cost share would potentially double, significantly increasing the plant CAPEX and so the system LCOS.

Regarding the storage media cost, its contribution is negligible for the cold storage system while it is relevant for the hot one. This is due to the high cost of the Therminol VP1, which consists of 97.5% of the hot storage HTF cost, demonstrating the importance of reducing the amount of Therminol VP1 needed by employing cheap solid materials (rocks-like) as storage media.



**Figure 8** Cost shares and total cost of the optimal system for the input variables of Table 1

Finally, the resulting LCOS as a function of the price of purchased electricity ( $p_{el}$ ) and number of full cycles per year is reported in **Figure 9**. As the storage duration is assumed at 10h in this work, a single complete charge/discharge cycle lasts 20h, and, for example, 350 cycles per year corresponds to 7000h of operation per year.

The LCOS decreases with an increase in the number of annual cycles, and increases with the increase of  $p_{el}$ . In particular, for an electricity price of 0.03 €/kWh and 300 full cycles per year, an LCOS of 0.147 €/kWh is evaluated.

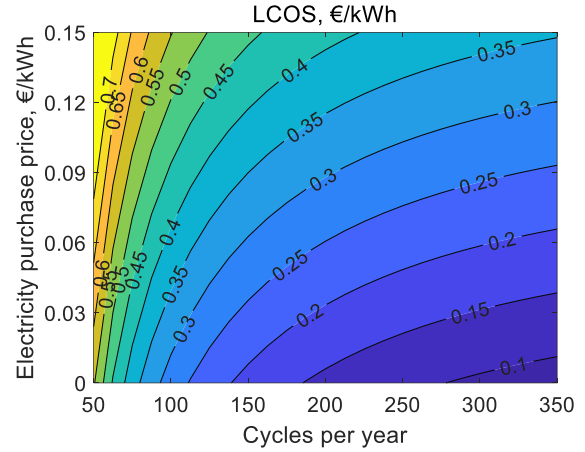


**Figure 9** LCOS [€/kWh] of the optimal system for the input variables of Table 1 as a function

### 5.1. Effect of temperature difference between the two phases across the PHE

As already mentioned in the previous section, a large share of the system cost is related to the heat exchangers of the cold and hot storage (64% of the total system cost). This last term can be greatly reduced by increasing the difference between the charging and discharging phase CO<sub>2</sub> temperature profiles in the PHE, defined as  $\Delta T_{ch-dh\ HOT\ TES}$ , as its increment directly leads to a reduction of the heat exchangers surfaces. The effect of increasing this parameter from 10°C to 20°C can be understood comparing **Figure 7** with **Figure 10**. The second figure, with  $\Delta T_{ch-dh\ HOT\ TES}$  of 20°C, also evidences again that the optimizer tends to maximize the Therminol VP1 temperature difference at the expenses of a more pinched heat exchanger. Since increasing the oil  $\Delta T$  reduces the amount of HTF required, that has a relevant importance on the total costs, the optimizer aims at reducing it at the cost of a more expensive HX. On the other hand, as the cost of water is negligible compared to the HX cost, the first thermal loop is optimized to maximize the internal  $\Delta T$ .

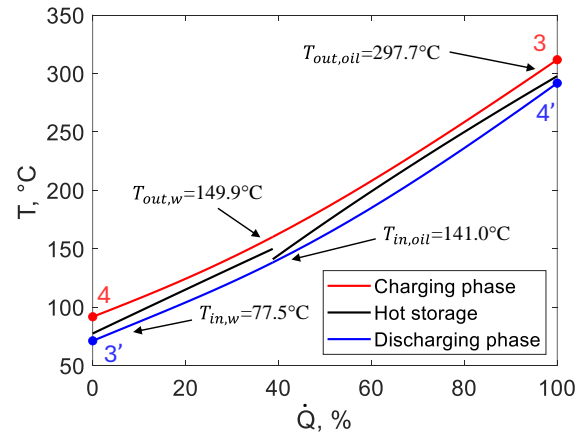


**Figure 10** T-Q diagram of the optimal configuration of the hot storage system for a  $\Delta T_{ch-dh\ HOT\ TES}$  of 20°C

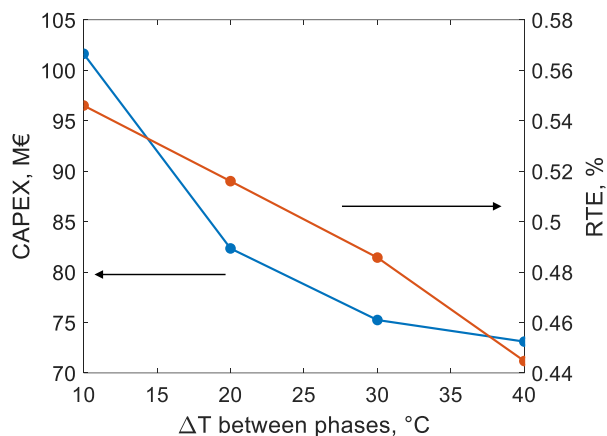


**Figure 11** System CAPEX and RTE as a function of  $\Delta T_{ch-dh\ HOT\ TES}$

As result the increase in  $\Delta T_{ch-dh\ HOT\ TES}$  brings to a reduction of costs but also reduces the Carnot battery RTE, since a lower turbine inlet temperature in the discharging phase ( $T_4'$ ) can be achieved for the same maximum charging temperature ( $T_3$ ) as reported in **Figure 11**.

The system sensitivity to  $\Delta T_{ch-dh\ HOT\ TES}$  shows opposing effects on the LCOS, as it is directly proportional to the system CAPEX and inversely proportional to its RTE. To visualize this tradeoff, **Figure 12** reports the system LCOS as function of the number of annual cycles for different values of  $\Delta T_{ch-dh\ HOT\ TES}$ , by assuming an electricity purchase price of 0.03 €/kWh.

All cases show quite comparable values of LCOS at constant number of cycles per year, with the best cases being the ones characterized by a  $\Delta T_{ch-dh\ HOT\ TES}$  of 20°C and 30°C. In particular, for a limited number of annual cycles, 30°C is a preferable value because it leads to slightly lower LCOS. On the other hand, increasing the number of cycles per year, the improvement of RTE for the case with  $\Delta T_{ch-dh\ HOT\ TES}$  of 20°C allows to obtain lower LCOS.

Differently, increasing the minimum temperature difference at the cold storage heat exchanger leads to a such important drop of system RTE that in turn always leads to an increase of LCOS.

Nevertheless, it must be noted that, according to the thermodynamic results of this work and the economic assumptions of **Table 3**, the variation in LCOS for different  $\Delta T_{ch-dh\ HOT\ TES}$  values falls within the uncertainty range of the employed cost correlations and a more detailed cost analysis or a slightly different set of assumptions could yield different outcomes.

## 6. CONCLUSIONS

In this work a methodology for the optimization of transcritical CO<sub>2</sub> Carnot batteries based on a dual-loop hot storage system has been presented, considering shared heat exchangers between the charging and the discharging phases.

The proposed methodology consists of two steps: first, the charging and discharging cycles are optimized to maximize the system RTE based on a given set of design variables; second, the

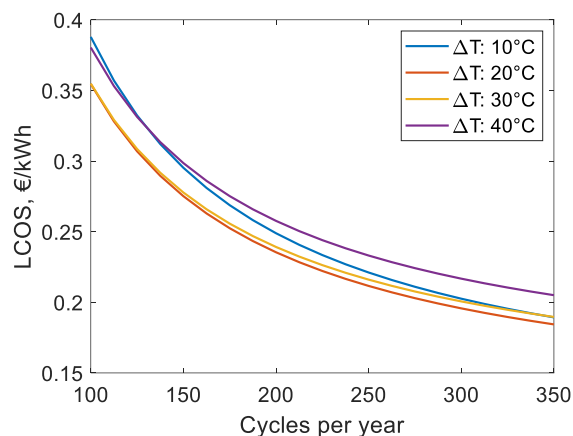


**Figure 12** System LCOS as a function of the  $\Delta T_{ch-dh\ HOT\ TES}$  and the number of annual cycles for  $p_{el}=0.03$  €/kWh

hot storage system configuration is optimized to minimize its investment cost. The methodology presented was then applied to optimize a system under reasonable boundary conditions, aligned with the state of the art of its components.

An optimal RTE of 54.6% was achieved, with a maximum temperature of 293.8°C in the charging phase and a maximum pressure of 250 bar. Results suggested that the largest share of the capital cost is related to the storage systems, while the heat pump and power cycle equipment accounts for around 12%-14% of the total investment, thus supporting the choice to firstly optimize the system RTE and then minimize the hot TES section from an economic perspective.

Additionally, it is highlighted that the heat exchangers related to the hot and to the cold storage represent a great share of the costs, proving the need to adopt shared heat exchangers heat pump and power cycle modes.

Finally, the LCOS of the selected configuration has been evaluated for different scenarios of electricity price and number of annual charging and discharging cycles, leading to LCOS in the range from 0.2 to 0.4 €/kWh, depending on the market and system operation assumptions.

Lastly, an analysis on the effect of the minimum difference between the CO<sub>2</sub> temperature profiles of the charging and discharging phase at the hot storage ( $\Delta T_{ch-dh\ HOT\ TES}$ ) was carried out. Increasing the value of  $\Delta T_{ch-dh\ HOT\ TES}$  leads to a decrease in both the system CAPEX and RTE, thus leading to a trade-off on the LCOS. In particular, for a lower number of annual cycles, higher  $\Delta T_{ch-dh\ HOT\ TES}$  are preferable while the opposite is true for a higher number of annual cycles.

Future works will focus on increasing the number of case studies and sensitivity analysis to strengthen the system optimization. In particular, different pressure levels, storage size, different heat exchangers configuration and design assumptions will be considered as additional optimization variables.

## NOMENCLATURE

### Acronyms

BESS	Battery Energy Storage Systems
CAES	Compressed Air Energy Storage
CAPEX	Capital Expenditure
HTC	Heat transfer Coefficient
HTF	Heat Transfer Fluid
HX	Heat Exchanger
LAES	Liquid Air Energy Storage
LCOS	Levelized Cost Of Storage
LDES	Long Duration Energy Storage
PCHE	Printed Circuit Heat Exchanger
PHE	Primary Heat Exchanger
PHS	Pumped Hydro Storage
PTES	Pumped Thermal Energy Storage
RTE	Round Trip Efficiency
TES	Thermal Energy Storage
VRES	Variable Renewable Energy Sources

### Symbols

$\Delta T$	Temperature difference (°C)
$\Delta P$	Pressure drop (bar)
$W$	Mechanical energy (J)
$Q$	Thermal energy (J)
$\dot{Q}$	Thermal power (W)
$p$	Pressure (bar)
$T$	Temperature (°C)
$s$	Specific entropy (kJ/kg K)
$\dot{m}$	Mass flow rate (kg/s)

### Subscripts

<i>ch</i>	Charging phase (Heat Pump)
<i>dh</i>	Discharging phase (Power Cycle)
<i>cold</i>	Cold storage

## ACKNOWLEDGEMENTS

This study was carried out within the NEST - Network 4 Energy Sustainable Transition (D.D. 1243 02/08/2022, PE00000021) and received funding under the National Recovery and Resilience Plan (NRRP), Mission 4 Component 2 Investment 1.3, funded from the European Union - NextGenerationEU. This manuscript reflects only the authors' views and opinions, neither the European Union nor the European Commission can be considered responsible for them.

This paper was carried out within the project HICLOPS "High-medium temperature closed power cycles for waste heat recovery and renewable sources" that has received funding from the MUR Progetti di Rilevante Interesse Nazionale (PRIN) Bando 2022 under grant No 2022HMZ39A.

## REFERENCES

- [1] CAISO, 'Managing the evolving grid'. Accessed: Nov. 11, 2024. [Online]. Available: <https://www.caiso.com/about/our-business/managing-the-evolving-grid>
- [2] International Energy Agency, 'Will more wind and solar PV capacity lead to more generation curtailment?' Accessed: Nov. 11, 2024. [Online]. Available: <https://www.iea.org/reports/renewable-energy-market-update-june-2023/will-more-wind-and-solar-pv-capacity-lead-to-more-generation-curtailment>
- [3] U. Akram, M. Nadarajah, R. Shah, and F. Milano, 'A review on rapid responsive energy storage technologies for frequency regulation in modern power systems', *Renewable and Sustainable Energy Reviews*, vol. 120, p. 109626, Mar. 2020, doi: 10.1016/j.rser.2019.109626.
- [4] M. M. Rahman, A. O. Oni, E. Gemechu, and A. Kumar, 'Assessment of Energy Storage technologies: a Review', *Energy Conversion and Management*, vol. 223, 2020, doi: 10.1016/j.enconman.2020.113295.
- [5] B. E. Lebrouhi, S. Baghi, B. Lamrani, E. Schall, and T. Kousksou, 'Critical materials for electrical energy storage: Li-ion batteries', *Journal of Energy Storage*, vol. 55, p. 105471, Nov. 2022, doi: 10.1016/j.est.2022.105471.
- [6] Hydrostor, 'Willow Rock Energy Storage Center', Hydrostor.ca. Accessed: Jan. 01, 2024. [Online]. Available: <https://hydrostor.ca/projects/willow-rock-energy-storage-center/>
- [7] Highview Power, 'Ongoing Projects', highviewpower.com. Accessed: Jan. 01, 2024. [Online]. Available: <https://highviewpower.com/projects/#uk-projects>
- [8] 'Electro-thermal Energy Storage (MAN ETES)', MAN Energy Solutions. Accessed: Jan. 01, 2023. [Online]. Available: <https://www.man-es.com/energy-storage/solutions/energy-storage/electro-thermal-energy-storage>
- [9] 'ETES System Overview | Echogen Power Systems', www.echogen.com. Accessed: Jan. 01, 2023. [Online]. Available: <https://www.echogen.com/energy-storage/etes-system-overview/>
- [10] Westinghouse Electric Company, 'Westinghouse LDES', westinghousenuclear.com. Accessed: Jan. 01, 2024. [Online]. Available: <https://info.westinghousenuclear.com/news/westinghouse-long-duration-energy-storage-solution-selected-for-department-of-energy-program-in-alaska>
- [11] M. Mercangöz, J. Hemrle, L. Kaufmann, A. Z'Graggen, and C. Ohler, 'Electrothermal energy storage with transcritical CO<sub>2</sub> cycles', *Energy*, vol. 45, no. 1, pp. 407–415, Sep. 2012, doi: 10.1016/j.energy.2012.03.013.
- [12] M. Morandin, F. Maréchal, M. Mercangöz, and F. Buchter, 'Conceptual design of a thermo-electrical energy storage system based on heat integration of thermodynamic cycles – Part A: Methodology and base case', *Energy*, vol. 45, no. 1, pp. 375–385, Sep. 2012, doi: 10.1016/j.energy.2012.03.031.
- [13] F. Ayachi, N. Tauveron, T. Tartière, S. Colasson, and D. Nguyen, 'Thermo-Electric Energy Storage involving CO<sub>2</sub> transcritical cycles and ground heat storage', *Applied Thermal Engineering*, vol. 108, pp. 1418–1428, Sep. 2016, doi: 10.1016/j.applthermaleng.2016.07.063.

- [14] C. K. Ho, M. Carlson, P. Garg, and P. Kumar, 'Technoeconomic Analysis of Alternative Solarized s-CO<sub>2</sub> Brayton Cycle Configurations', *Journal of Solar Energy Engineering*, vol. 138, no. 051008, Jul. 2016, doi: 10.1115/1.4033573.
- [15] V. Dostal, M. J. Driscoll, P. Hejzlar, and N. E. Todreas, 'A Supercritical CO<sub>2</sub> Gas Turbine Power Cycle for Next-Generation Nuclear Reactors', in *10th International Conference on Nuclear Engineering, Volume 2*, Arlington, Virginia, USA: ASME/EDC, Jan. 2002, pp. 567–574. doi: 10.1115/ICONE10-22192.
- [16] M. Astolfi, 'An innovative approach for the technoeconomic optimization of organic Rankine cycles', Mar. 2014, Accessed: Nov. 25, 2024. [Online]. Available: <https://www.politesi.polimi.it/handle/10589/89363>
- [17] D. W. Lee and A. Sharma, 'Melting of ice slurry in a tube-in-tube heat exchanger', *Int. J. Energy Res.*, vol. 30, no. 12, pp. 1013–1021, Oct. 2006, doi: 10.1002/er.1204.
- [18] M. Kauffeld, M. J. Wang, V. Goldstein, and K. E. Kasza, 'Ice slurry applications', *International Journal of Refrigeration*, vol. 33, no. 8, pp. 1491–1505, Dec. 2010, doi: 10.1016/j.ijrefrig.2010.07.018.
- [19] P. W. Egolf and M. Kauffeld, 'From physical properties of ice slurries to industrial ice slurry applications', *International Journal of Refrigeration*, vol. 28, no. 1, pp. 4–12, Jan. 2005, doi: 10.1016/j.ijrefrig.2004.07.014.
- [20] R. Span and W. Wagner, 'A New Equation of State for Carbon Dioxide Covering the Fluid Region from the Triple-Point Temperature to 1100 K at Pressures up to 800 MPa', *Journal of Physical and Chemical Reference Data*, vol. 25, no. 6, pp. 1509–1596, 1996, doi: 10.1063/1.555991.
- [21] Z. Liu and R. H. S. Winterton, 'A General Correlation for Saturated and Subcooled Flow Boiling in Tubes and annuli, Based on a Nucleate Pool Boiling Equation', *International Journal of Heat and Mass Transfer*, vol. 34, no. 11, pp. 2759–2766, 1991, doi: 10.1016/0017-9310(91)90234-6.
- [22] L. Friedel, 'Improved Friction Pressure Drop Correlation for Horizontal and Vertical Two-Phase Pipe Flow', *European Two-Phase Flow Group Meeting*, pp. 485–492, 1979.
- [23] A. Cavallini *et al.*, 'Condensation in Horizontal Smooth Tubes: a New Heat Transfer Model for Heat Exchanger Design', *Heat Transfer Engineering*, vol. 27, no. 8, pp. 31–38, 2006, doi: 10.1080/01457630600793970.
- [24] V. Gnielinski, 'New equations for heat and mass transfer in turbulent pipe and channel flow', *International Chemical Engineering*, vol. 16, no. 2, pp. 359–368, 1976.
- [25] N. H. Chen, 'An Explicit Equation for Friction Factor in Pipe', *Industrial & Engineering Chemistry Fundamentals*, vol. 18, no. 3, pp. 296–297, 1979, doi: 10.1021/i160071a019.
- [26] D. Alfani, A. Giostri, and M. Astolfi, 'Working Fluid Selection and Thermodynamic Optimization of the Novel Renewable Energy-Based RESTORE Seasonal Storage Technology', *Journal of Engineering for Gas Turbines and Power*, vol. 146, no. 101013, May 2024, doi: 10.1115/1.4065407.
- [27] MATLAB, 'Global Optimization Toolbox User's Guide', Sep. 2024, Accessed: Feb. 25, 2025. [Online]. Available: [https://www.mathworks.com/help/pdf\\_doc/gads/gads.pdf](https://www.mathworks.com/help/pdf_doc/gads/gads.pdf)
- [28] 'Cost of Current Cooling Technologies', Enersion. Accessed: Feb. 25, 2025. [Online]. Available: <https://enersion.com/tips-tricks/cost-of-current-cooling-technologies/>
- [29] S. Mazzoni, J. Y. Sze, B. Nastasi, S. Ooi, U. Desideri, and A. Romagnoli, 'A techno-economic assessment on the adoption of latent heat thermal energy storage systems for district cooling optimal dispatch & operations', *Applied Energy*, vol. 289, p. 116646, May 2021, doi: 10.1016/j.apenergy.2021.116646.
- [30] N. T. Weiland, B. W. Lance, and S. R. Pidaparti, 'sCO<sub>2</sub> Power Cycle Component Cost Correlations From DOE Data Spanning Multiple Scales and Applications', in *Volume 9: Oil and Gas Applications; Supercritical CO<sub>2</sub> Power Cycles; Wind Energy*, Phoenix, Arizona, USA: American Society of Mechanical Engineers, Jun. 2019. doi: 10.1115/GT2019-90493.
- [31] M. D. Carlson, B. M. Middleton, and C. K. Ho, 'Techno-Economic Comparison of Solar-Driven sCO<sub>2</sub> Brayton Cycles Using Component Cost Models Baselined With Vendor Data and Estimates', in *ASME 2017 11th International Conference on Energy Sustainability*, Charlotte, North Carolina, USA: American Society of Mechanical Engineers, Jun. 2017, p. V001T05A009. doi: 10.1115/ES2017-3590.
- [32] G. Manzolini, G. Lucca, M. Binotti, and G. Lozza, 'A two-step procedure for the selection of innovative high temperature heat transfer fluids in solar tower power plants', *Renewable Energy*, vol. 177, pp. 807–822, Nov. 2021, doi: 10.1016/j.renene.2021.05.153.
- [33] J. D. McTigue, P. Farres-Antunez, K. S. J, C. N. Markides, and A. J. White, 'Techno-economic analysis of recuperated Joule-Brayton pumped thermal energy storage', *Energy Conversion and Management*, vol. 252, p. 115016, Jan. 2022, doi: 10.1016/j.enconman.2021.115016.

# DuEPublico

Duisburg-Essen Publications online

UNIVERSITÄT  
DUISBURG  
ESSEN

*Offen im Denken*

ub

universitäts  
bibliothek

*Published in: 6th European Conference on Supercritical CO<sub>2</sub> (sCO<sub>2</sub>) for Energy Systems*

This text is made available via DuEPublico, the institutional repository of the University of Duisburg-Essen. This version may eventually differ from another version distributed by a commercial publisher.

**DOI:** 10.17185/duepublico/83300

**URN:** urn:nbn:de:hbz:465-20250428-121857-0



This work may be used under a Creative Commons Attribution 4.0 License (CC BY 4.0).